Fabian Habicht, Fatma Cansu Yücel, Mohammad Rezay Haghdoost, Kilian Oberleithner, Christian Oliver Paschereit

Acoustic modes in a plenum downstream of a multitube pulse detonation combustor

Acoustic Modes in a Plenum Downstream of a Multi-tube Pulse Detonation Combustor

Fabian Habicht *, Fatma Cansu Yücel †, Mohammad Rezay Haghdoost ‡, Kilian Oberleithner §
and Christian Oliver Paschereit ¶
Institute of Fluid Dynamics and Technical Acoustics, Technische Universität Berlin, 10623 Berlin, Germany

The operation of a multi-tube pulse detonation combustor (PDC) evokes undesirable pressure fluctuations for a turbine downstream of the combustor. Pressure measurements in a downstream annular plenum reveal distinct pressure fluctuations. While the pressure peaks due to the shock waves emanating from the PDC tubes have been investigated in previous studies, pressure oscillations throughout the remaining cycle duration have received far less attention. Based on azimuthal and frequency mode decomposition of pressure signals at six circumferential positions, these oscillations are found to result from acoustic modes that are excited by PDC operation. This conclusion is verified by comparison with numerically calculated eigenmodes of the plenum. The impact of different operating parameters as well as the plenum outlet geometry on the acoustic oscillations are determined. The sequential firing of the PDC tubes at the lowest firing frequency in combination with a small blockage ratio was identified as the favorable configuration for the smallest acoustic fluctuations.

Nomenclature

β	=	blockage ratio at the plenum outlet
γ	=	isentropic coefficient
ζ	=	non-dimensional frequency
φ	=	equivalence ratio
θ	=	azimuthal coordinate
Ψ	=	acoustic eigenmode
ω	=	oscillation frequency (Hz)
c	=	speed of sound (m/s)
f	=	frequency (Hz)
j	=	PDC tube number
L	=	axial length of the plenum (m)
l	=	longitudinal mode number
m	=	azimuthal mode number
N	=	number of PDC tubes
n	=	number of simultaneously operated PDC tubes
p	=	pressure (bar)
R_s	=	specific gas constant (J/(kg K))
r	=	radial coordinate (m)
T	=	temperature (K)
t	=	time (s)
u	=	propagation velocity (m/s)
x	=	axial coordinate (m)

*Graduate Research Assistant (PhD Student), Chair of Fluid Dynamics, Corresponding author: fabian.habicht@tu-berlin.de
†Graduate Research Assistant (PhD Student), Chair of Fluid Dynamics
‡Graduate Research Assistant (PhD Student), Laboratory for Flow Instabilities and Dynamics
§Professor, Laboratory for Flow Instabilities and Dynamics
¶Professor, Chair of Fluid Dynamics

I. Introduction

Pressure gain combustion (PGC) has received increasing attention in the last decades due to its potential of achieving a significant gain in thermal efficiency of gas turbines. Numerous research groups invested enormous efforts for investigating different concepts, such as pulse jet, pulse detonation combustor (PDC), rotating detonation combustor (RDC) [1], and shockless explosion combustor (SEC) [2]. All concepts are based on a periodic combustion process that results in pulsating flow conditions at the combustor outlet. These fluctuations are especially pronounced downstream of a PDC, where propagating detonations ultimately result in shock waves exiting the combustor [3]. However, at the inlet of conventional turbines, steady flow conditions are favorable to ensure good performance and reduced mechanical stress. This was verified experimentally by Rouser et al. [4], who found that the periodic fluctuations in the flow field downstream of a PDC lead to a significant decrease in the cycle-averaged turbine efficiency. Hence, minimizing pressure fluctuation downstream of a PDC is a major challenge for realizing its integration into a gas turbine.

Two approaches have been proposed to reduce pressure fluctuations at the turbine inlet downstream of a PDC: adjusting the operation parameters, such as firing frequency and firing pattern, and integrating a plenum upstream of the turbine [5, 6]. Experiments conducted by Rouser et al. [4] revealed a decrease in the amplitude of the observed pressure fluctuations with increasing firing frequency resulting in an increase in turbine efficiency. The operation frequency of a PDC, however, is limited, which restricts the potential of this approach. Experimental investigations of a hybrid multi-tube PDC conducted by Rasheed et al. [7] suggest the optimization of the firing pattern as an alternative concept for the attenuation of pressure fluctuations. They found a substantial decrease in the measured peak pressure downstream of the PDC outlet when applying a sequential firing pattern compared to a simultaneous operation of all PDC tubes. Moreover, experimental investigations by Qiu et al. [8] revealed that asynchronous firing of two PDC tubes allows for increasing the specific work extracted by a turbine compared to a synchronous firing pattern. In a recent study conducted by Haghdoost et al. [6], an annular plenum was attached to a PDC with six circumferentially distributed tubes. The measured pressure amplitudes revealed successful attenuation of the shock waves exiting the PDC tubes along the axis of the plenum. Applying sequential firing led to a further improved attenuation of the shock waves compared to firing of a single PDC tube. Thus, combining all three approaches could lead the way for a substantial attenuation of the amplitude in pressure fluctuations at the turbine inlet.

All studies mentioned above focus on the maximum pressure amplitude resulting from the shock wave associated with the propagating detonation in the PDC tubes. Besides this peak amplitude, measurements in the scope of this work revealed considerable pressure oscillations in the attached annular plenum in the time between the firing of PDC tubes. Pulsating inflow conditions for conventional turbines can result in significant reduction of turbine efficiency due to different phenomena such as incident angle, variable blade loading and passage vortex formation [9–12]. Hence, mitigation of pressure fluctuations is crucial to maintain the efficiency gain provided by the pressure gain combustion.

In this work, measured pressure traces are examined with respect to acoustic eigenmodes in order to shed some light on the shape and excitation mechanisms of pressure oscillations in a generic plenum. The shape and the oscillation frequency of excited modes are extracted from measurement data by modal decomposition of pressure signals at various azimuthal positions, as proposed by Evesque et al. [13] or Noiray and Schuermans [14]. Besides, numerical solution of the acoustic Helmholtz equation as proposed by Mensah et al. [15] are conducted to identify the acoustic eigenmodes of the plenum. Further, the acoustic energy of pressure oscillations are evaluated as a function of PDC operation parameters, i.e., firing pattern and firing frequency, as well as the blockage ratio at the plenum outlet. The blockage represents a fundamental design parameter for the transition section between the plenum and an attached turbine. The conducted investigations on the influence of operation parameters of the multi-tube PDC and the blockage ratio on the energy level, amplitude and number of excited acoustic modes may contribute to achieve suitable inflow conditions for an attached turbine, and thereby increase the overall gas turbine efficiency.

II. Methodology

First, the experimental setup is presented followed by the measurement procedure. Subsequently, signal processing methods are introduced allowing for the examination of pressure oscillations in the plenum based on pressure signals at multiple axial and azimuthal positions. Lastly, a numerical method for the prediction of acoustic eigenmodes and eigenfrequencies is presented. These calculations will help to interpret the results obtained from the measurements.

A. Experimental Setup

A PDC test-rig consisting of six tubes and a plenum arranged in a can-annular configuration was used for this investigation (Fig. 1). The valveless design of the air supply ensured a constant air mass flow rate, which was closed-loop

controlled to a steady-state value of 900 kg/h by an electro-hydraulic proportional valve in combination with a Coriolis mass flow meter. The air flow was separated upstream of the test rig by a manifold to six lines, each feeding the air plenum of one PDC tube with an air mass flow rate of 150 kg/h, respectively. To hinder pressure waves and hot exhaust gases from reaching the air plenum, the air flow was choked upstream of the fuel injection. Hydrogen, which was used as fuel, was injected into each PDC tube by three high-speed solenoid valves, respectively. An upstream installed dome-loaded pressure regulator assured fast adjustment of a constant supply pressure during the fuel injection resulting in a nearly constant fuel mass flow rate. This allowed for the injection of a fuel–air mixture at nearly constant equivalence ratio throughout the injection period. The supply pressures of fuel and oxidizer were monitored by two static pressure sensors.

Mixing tubes were installed to guide the mixture to three injection ports while enhancing the mixing of fuel and oxidizer. The injection ports were distributed circumferentially close to the planar upstream end wall of each PDC tube. A spark plug was located in the center of the end wall to allow for controlled ignition of the mixture when the injection was completed. The ignition spark was triggered 4 ms subsequent to the fuel valve closing. By this, an air buffer was injected before ignition allowing for minimizing the fuel concentration inside the mixing tubes. This procedure reduces mechanical and thermal stress on the mixing geometry.

Subsequent to ignition, a deflagration propagates through the PDC tube. Due to stretching of the flame surface caused by turbulence and expansion of hot combustion products, the flame accelerates and eventually undergoes a deflagration-to-detonation transition (DDT). This process was accelerated by the installation of a series of five orifice plates with a blockage ratio of 0.43 each, equally spaced at 85 mm. The detonation that is initiated in the DDT section of 0.5 m length subsequently propagates through the detonation tube with a length of 0.9 m and an inner tube diameter of 30 mm. Three piezoelectric pressure sensors were installed in PDC tube 1 to detect the arrival time of the detonation wave. A coated thermocouple (type K) was installed in PDC tube 5 to allow for monitoring the gas temperature.

The outlets of the PDC tubes were equipped with a divergent nozzle increasing the cross section area by the factor of 2.25, which are used to provide a smoother diffraction of the shocks exiting the PDC. The six PDC tubes were attached to an annular plenum in a can-annular configuration on a pitch-circle diameter of 260 mm. The radial dimension of the annular duct of 130 mm matched the distance of two neighboring PDC tubes. The plenum had an axial length of $L = 500$ mm with $x = 0$ mm at the inlet area. Five piezoresistive pressure sensors were mounted at the outer wall of the plenum equally spaced along the axial direction at the circumferential position of PDC tube 5. Additionally, five piezoelectric pressure sensors were installed circumferentially at $x/L = 0.14$ downstream of the other PDC tubes. Further five sensors were mounted at equal azimuthal positions at $x/L = 0.86$. The circumferential and radial positions of the pressure sensors are shown in Fig. 2a. All sensors were flush mounted to the plenum outer wall at $r_o = 196$ mm, while their circumferential location θ_j match the azimuthal position of PDC tube j.

B. Measurement Procedure

As shown by Haghdoost et al. [6], pressure fluctuations at the outlet of the annular plenum depend on the operation of the multi-tube PDC. Besides, pressure oscillations are expected to be effected by the acoustic boundary condition at

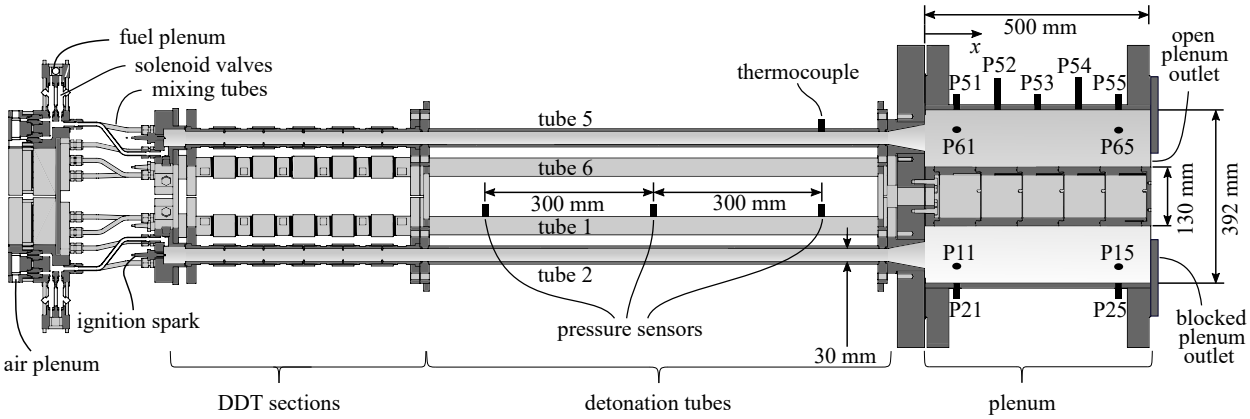

Fig. 1 Sketch of a cross section of the PDC test rig consisting of six circumferentially arranged tubes, common supply lines for air and fuel, and an annular plenum.

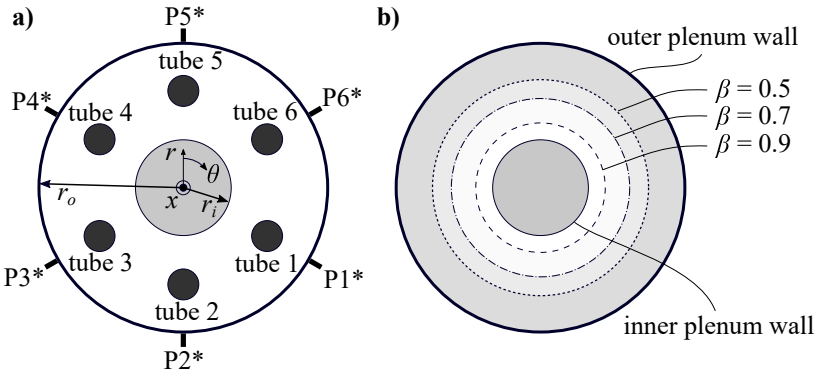

Fig. 2 Cross section (a) and rear view (b) of the annular plenum. The dimensions of the applied orifice plates are visualized in (b).

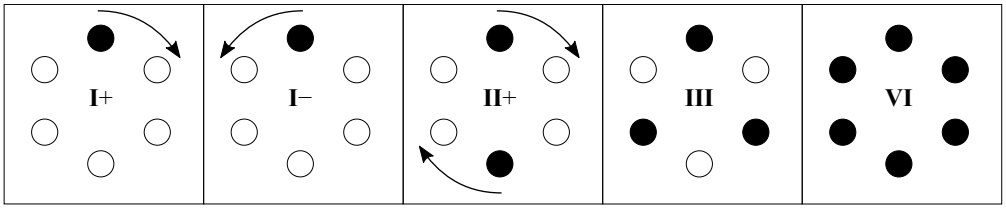

Fig. 3 Firing patterns. I+ and I−: sequential firing with alternate direction of rotation, II+: simultaneous firing of two PDC tubes, III: alternate firing of three simultaneously firing PDC tubes, and VI: simultaneous firing of all six PDC tubes.

the plenum outlet. Therefore, three parameters were varied in the scope of this work to evaluate their effect on pressure oscillations in the annular plenum: the blockage ratio β of the plenum outlet, the firing frequency f_{tube}, and the firing pattern. To allow for variation of the acoustic boundary condition of the annular plenum, orifice plates were mounted at the outlet. The inner diameter of the orifices was varied to allow for the application of four blockage ratios, as visualized in Figure 2b: 0, 0.5, 0.7, and 0.9. The injection period was set to a constant value of 21 ms, which resulted in completely filled PDC tubes before ignition. By varying the cycle duration between 30 and 90 ms, the duty cycle of the injection valves was varied from 0.23 to 0.7. By this, the firing frequency f_{tube}, which denotes the operation frequency of a single PDC tube, was varied from 11.1 to 33.3 Hz. Besides the firing frequency, the firing pattern defines the succession of pressure pulses entering the plenum. Five different patterns, illustrated in Fig. 3, were applied: sequential firing (**I**), simultaneous firing of two PDC tubes (**II**), the alternate firing of three simultaneously operating tubes (**III**), and simultaneous firing of all six PDC tubes (**VI**). The naming convention is based on the number of PDC tubes operated simultaneously. For sequential firing, the rotation direction is varied between positive (**I+**) and negative (**I−**) azimuthal direction. These firing patterns result in various effective firing frequencies f_{eff}, given by

$$f_{\text{eff}} = \frac{N}{n} f_{\text{tube}} \tag{1}$$

with the total number of PDC tubes N and the number of tubes that are operated simultaneously n. In this work $N = 6$ holds for all measurements. The value of f_{eff} denotes the frequency at which shocks from any PDC tube enter the plenum. For each applied parameter combination of β, f_{tube}, and the firing pattern, the PDC tubes were operated for ten cycles. This number was found to be sufficient to obtain repeatable pressure signals for all installed sensors.

During the operation of the PDC, fuel needs to be added periodically to the continuous air flow. As a consequence, the fuel mass flow rate $\dot{m}_{\text{fuel}}$ in the supply line fluctuates, which could only be measured time-averaged by a Coriolis mass flow meter due to limited sample rate. However, the time-resolved fuel mass flow rate $\dot{m}_{\text{fuel}}$ could be determined from the measured static pressure in the supply line. A linear calibration between supply pressure and mass flow rate was extracted from preliminary experiments with continuous fuel flow at various flow rates. Examination of the time-averaged measured fuel supply pressure during the injection period revealed that the pressure decreased with increasing firing frequency. We explain this by the behavior of the dome-loaded pressure regulator that was charged

with a dome pressure of 5 bar for all conducted experiments. The number of open valves changes over time as a function of the number of tubes that are filled simultaneously, which depends on the firing pattern and the firing frequency. When the number of open valves increases, the static pressure upstream of the valves decreases almost instantaneously. Due to unavoidable inertia of the pressure regulator, a temporary mismatch between the target pressure of 5 bar and the actual supply pressure was observed. Thus, the time-averaged measured fuel supply pressure deviates slightly from the set value. When increasing the firing frequency, the mentioned event of a change in the number of open valves occurs more frequently. Since the response time of the pressure regulator does not change, the time of decreased supply pressure relative to the cycle duration increases. Therefore, the time-averaged fuel supply pressure during the injection period decreases with increasing firing frequency. This ultimately results in a decrease in equivalence ratio in the PDC tubes, which has to be considered when evaluating the effect of the firing frequency on the pressure oscillations in the plenum. For all measurements, a cycle-to-cycle standard deviation of the fuel supply pressure of roughly 1 % was observed, indicating a high repeatability of reactant injection. Furthermore, it should be noted that no significant increase of static pressure in the plenum was observed for any applied blockage ratio. Thus, the blockage ratio has no effect on the fuel supply.

C. Signal Processing

In this work, acoustic pressure oscillations in the annular plenum are examined. First, the detonation velocity in the PDC tubes is determined, which defines the pressure amplitude of shocks entering the plenum. Subsequently, the pressure signals in the plenum are analyzed with respect to the occurrence of acoustic modes.

The detonation velocity is calculated from the time-of-flight Δt_{tof} between the detection of the shock associated to the detonation wave in the sensors in PDC tube 1 by

$$u_{\mathrm{det}} = \frac{\Delta x}{\Delta t_{\mathrm{tof}}} - u_{\mathrm{flow}} \tag{2}$$

with the axial distance Δx between the sensors. The mean flow velocity u_{flow} of the injected mixture is determined from the initial thermodynamic conditions ($p_0 = 1$ atm and $T = 300$ K) and the mass flow rates of the mixture components. As a result of the cyclic PDC operation, the flow velocity changes periodically. Subsequent to the combustion event, a backflow of exhaust gases into the air supply is observed as indicated by a maximum pressure amplitude of 1 bar in the air plena. However, the applied purging duration of at least 5 ms was found to be sufficient to purge all exhaust gases from the combustor inlet section. Hence, the mixture flow velocity prior to the ignition event, can well be determined as described above. Comparing u_{det} to the Chapman–Jouguet (CJ) velocity allows for verifying that successful detonation initiation is achieved. The CJ velocity is determined from the initial thermodynamic state and the composition of the flammable mixture as proposed by Zeleznik et al. [16]. The equivalence ratio is assessed from the continuous air mass flow rate of 900 kg/h and the fuel mass flow rate, which is obtained from the linear correlation to the measured fuel supply pressure.

The operation of the multi-tube PDC results in substantial pressure fluctuations in pressure in the attached plenum. An example cycle-averaged pressure signal of sensor P55 is shown in Fig. 4 ($x/L = 0.86$, $\theta = 0$, $r = r_o$) for firing pattern **I+**, a firing frequency of 16.7 Hz, and a blockage ratio of 0.9. The largest pressure amplitude of roughly 0.9 bar is visible subsequent to firing of tube 5, which is located at the same circumferential position as sensor P55. The firing of the other PDC tubes results in pressure peaks of approximately 0.25 bar, respectively. Besides, pressure fluctuations can be observed throughout the entire operation time.

As mentioned above, the annular plenum was equipped with two arrays of circumferentially distributed pressure sensors, of which one was located at $x/L = 0.14$ and the other at $x/L = 0.86$. For each axial position the pressure signals of the six sensors are used to perform azimuthal frequency decomposition, which includes two subsequentially performed Fourier transforms (FTs), the first in azimuthal direction and the second in time. This methodology allows for the decomposition of the recorded pressure oscillations with respect to their frequency and their lag in phase between the sensors as the real part $\Re$ of complex harmonic oscillations according to

$$p\left(\theta, t\right) = \Re\left(\sum_{m=-\infty}^{\infty} \int_{-\infty}^{\infty} \hat{p}_m\left(\omega\right) e^{i\left(\omega t - m\theta\right)} \mathrm{d}\omega\right). \tag{3}$$

Here, $\hat{p}_m\left(\omega\right)$ denotes the spectrum of pressure amplitude as a function of the oscillation frequency $\omega = 2\pi f$. The index $m \in \mathbb{Z}$ denotes the azimuthal mode number that defines the number of pressure nodes along the circumference.

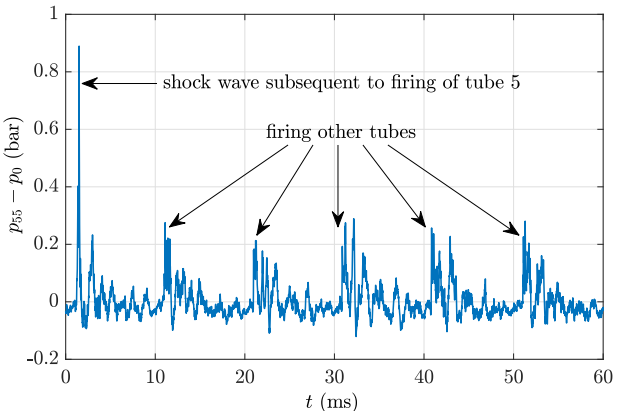

Fig. 4 Cycle-averaged pressure signal for sensor P55 with respect to atmospheric pressure conditions p_0 for firing pattern I+.

Since six pressure sensors were installed, spectra are obtained for $m \in [-2, -1, 0, +1, +2, 3]$. For $m = 0$, only pressure oscillations with all six sensors being in phase are considered. A positive value of m represents an acoustic mode that rotates in positive azimuthal direction with respect to θ. Negative azimuthal mode numbers result in an opposed rotation direction. The number of installed sensors allows for the determination of $\hat{p}_m$ up to a mode number of $m = 3$. For this value, the rotation direction cannot be extracted from the available data. Pressure oscillations with $|m| > 3$ cannot be resolved and are captured by spectra with lower values of m due to aliasing. However, only pressure oscillations with $|m| \leq 3$ are expected to establish as a result of the can-annular configuration of the six PDC tubes and the attached plenum.

In order to examine the energy contained in the different mode shapes, the obtained spectra $\hat{p}_m(f)$ are used to determine the power spectral density (PSD) by

$$\mathrm{PSD}_m(f) = \frac{1}{t_{\mathrm{meas}} f_{\mathrm{s}}^2} |\hat{p}_m^2(f)| \tag{4}$$

with the measurement duration t_{meas} and the sampling frequency $f_{\mathrm{s}} = 1\,\mathrm{MHz}$. Frequencies with $f < f_0$ are neglected, where

$$f_0 = f_{\mathrm{eff}} + 1/2\, f_{\mathrm{tube}}. \tag{5}$$

This results in pressure oscillations generated by propagating shock waves subsequent to the firing of the PDC tubes to be neglected while relevant acoustic oscillations remain unchanged. The presented methodology allows for the detailed evaluation of the recorded pressure signals in the annular plenum with respect to the shape and the frequency of excited acoustic modes as well as their respective energy.

D. Numerical Prediction of Acoustic Eigenmodes

Most of the observed pressure fluctuations in the plenum, shown in Fig. 4 at one distinct position, are assumed to arise from the excitation of acoustic modes. To verify this assumption, the spectra obtained from azimuthal frequency decomposition are compared to the predicted acoustic eigenmodes and eigenfrequencies, which are calculated by the numerical solution of the acoustic Helmholtz equation.

For acoustic pressure oscillations the ideal gas relation holds and the acoustic wave equation is given as

$$\nabla \cdot \left(c^2 \nabla p' \right) - \frac{\partial^2 p'}{\partial t^2} = 0, \tag{6}$$

with the vector differential operator ∇, the speed of sound c, and the pressure fluctuation p'. By assuming harmonic oscillation of the pressure fluctuations in time

$$p'\left(\vec{x}, t\right) = \hat{p}\left(\vec{x}\right) e^{i\omega t}, \tag{7}$$

the wave equation can be converted into the frequency domain, leading to a homogeneous Helmholtz equation

$$\nabla \cdot \left(c^2 \nabla \hat{p} \right) + \omega^2 \hat{p} = 0, \tag{8}$$

which denotes a linear eigenvalue problem with the complex pressure fluctuation amplitude $\hat{p}$, and the complex frequency of oscillation ω. Any solution of Eq. 8 can be written as a superposition of eigenvectors that can be interpreted as acoustic eigenmodes Ψ. Due to the axisymmetric geometry of the annular plenum, the eigenmodes can be written as

$$\Psi_{l,m}(x, r, \theta) = \tilde{\Psi}_{l,m}(x, r)\, e^{-im\theta}, \tag{9}$$

with l and m denoting the axial and circumferential mode number, respectively [17]. Generally, acoustic eigenmodes in an annular duct are also defined by the radial mode number. However, these modes were found to be associated with eigenfrequencies above 4 kHz for the investigated setup and no considerable amplitudes of pressure oscillations were observed in the experiments for these frequencies. Thus, only the axial and azimuthal modes $\Psi_{l,m}$ and their respective eigenfrequencies $\omega_{l,m}$ are investigated in the following. Both $\Psi_{l,m}$ and the respective eigenfrequency $\omega_{l,m}$ are complex numbers. The absolute value $|\Psi_{l,m}|$ represents the amplitude in pressure fluctuations, while its argument denotes the phase. For non-constant distribution of $|\Psi_{l,m}|$ along the circumference, two different oscillations modes can be observed depending on the excitation [18]. A standing mode is characterized by a constant phase and varying amplitude along the azimuthal coordinate θ. When the pressure waves rotate in the azimuthal direction, a constant amplitude and varying phase is observed along the circumference, which indicates a spinning mode. The oscillation frequency is given by the real part of $\omega_{l,m}$ as

$$f_{l,m} = \Re \left(\frac{\omega_{l,m}}{2\pi} \right), \tag{10}$$

while the imaginary part gives information on the growth rate of the associated pressure oscillation.

For the calculation of the acoustic eigenmodes, the finite element solver PyHoltz is used. This tool was developed at TU Berlin by Mensah et al. [19] for efficient computation of thermoacoustic modes and their dependence on variable parameters in annular combustion chambers. The walls of the plenum including the blocked outlet area are modeled as sound hard with the flow velocity fluctuations normal to the wall being forced to zero. The open outlet of the plenum is modeled as sound soft leading to a pressure node ($\hat{p} = 0$) at the outlet plane. The calculations were performed on an unstructured grid with a characteristic length of $l_c = 0.02$ m. Further reduction in l_c resulted in negligible changes in the calculated eigenfrequencies, which indicates that the chosen spatial resolution is sufficient for the present study. The application of Bloch's theory allows for reducing the domain to a wedge representing one sixth of the annular combustion chamber, which results in a significant improvement in the calculation time. The predicted eigenmodes and eigenfrequencies presented in this work were obtained from the numerical solution of the acoustic Helmholtz equation in the annular plenum without accounting for the PDC tubes. However, pressure oscillations in the plenum may interact with the PDC tubes. In order to quantify this effect, the acoustic eigenfrequencies were calculated for a geometry that includes the six PDC tubes. The results for both geometries agreed well in terms of eigenmodes and eigenfrequencies with a maximum deviation of 20 Hz in $f_{l,m}$.

The instrumentation of the test-rig does not allow for the measurement of the spatial distribution of the time-averaged gas temperature in the plenum, which is needed as an input parameter for the calculation of eigenmodes and eigenfrequencies. The time-averaged gas temperature close to the PDC outlet could, however, be extracted from the signal of the installed thermocouple in PDC tube 5 during the operation of the multi-tube PDC for 200 cycles. This operation duration allowed for convergence of the measured temperature to a steady-state value. The measured time-averaged gas temperature of 550 K, an isentropic coefficient of $\gamma = 1.4$ and a specific gas constant of $R_s = 287$J/(kg K) were applied as constant initial conditions for the solution of the acoustic Helmholtz equation.

The assumption of stationary and spatially constant gas properties of pure air in the plenum does not replicate the actual conditions in the experiments, as the PDC operation evokes the periodical occurrence of shock waves and the blowdown of combustion products. However, the measured pressure fluctuations shown in Fig. 4 indicate that the operation is predominated by small fluctuation with $p' \leq 0.1$ bar, which make up to 86 % of the operation time. Further, calculations assuming perfect mixture and thermodynamic equilibrium revealed only a maximum variation in the speed of sound of 3 % when accounting for the presence of combustion products. Therefore, the applied methodology is suitable of supporting the evaluation of pressure oscillations with reasonably small amplitude, as observed in the period between the peak pressures due to the firing of the PDC tubes. In order to accurately replicate the measured pressure oscillations in the annular plenum, modeling of the excitation by the firing of the PDC tubes would be needed, which is beyond the scope of this work.

III. Results and Discussion

In this section, the propagation velocities of the detonations inside the PDC tubes are evaluated for a blockage ratio of $\beta = 0.9$. The obtained detonation velocities, however, were found to be independent of β, which assures the following evaluation to hold for all applied acoustic boundary conditions. Subsequently, the numerical prediction of acoustic eigenmodes and the respective eigenfrequencies are presented and the azimuthal frequency decomposition of the measurement data is discussed. These examinations are performed for a blockage ratio of $\beta = 0.9$ and a firing frequency of $f_{\text{tube}} = 16.7$ Hz. The evaluation of measurement data from operation at differing firing frequencies and blockage ratios were found to result in qualitatively similar observations. Findings from the reference case ($\beta = 0.9$, $f_{\text{tube}} = 16.7$) are therefore transferable to all other settings, which are not shown for brevity. Lastly, a quantitative comparison of the acoustic pressure fluctuations for various operation parameters and acoustic boundary conditions is conducted.

A. Detonation Velocities

The propagation velocity of the detonation front u_{det} inside PDC tube 1 is analyzed as a function of the firing frequency. This velocity defines the pressure amplitude of the shock wave exiting the PDC tube. Thus, the value of u_{det} gives information on the excitation amplitude of pressure oscillations in the plenum. The cycle-averaged propagation velocity of the detonation is shown in Fig. 5a as a function of f_{tube} for a blockage ratio of $\beta = 0.9$.

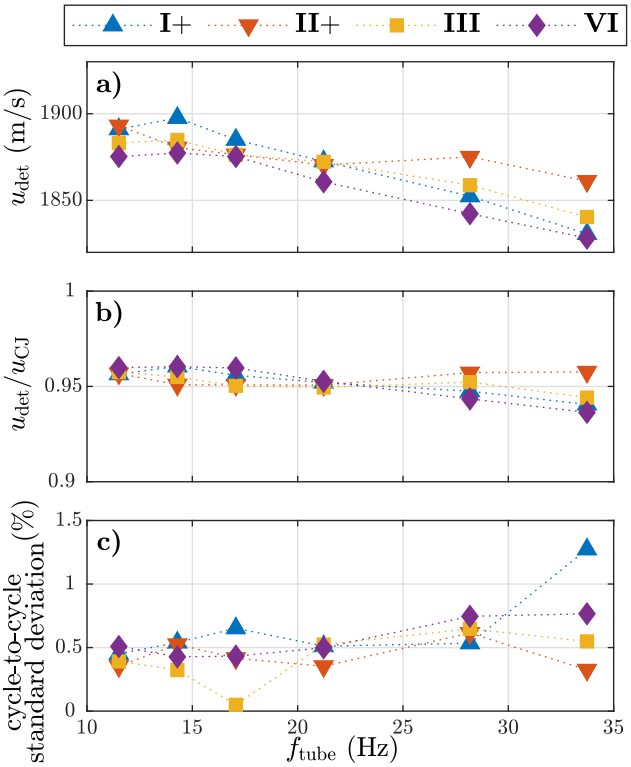

Fig. 5 Detonation velocities (a) normalized by the respective calculated CJ velocity (b) and the relative cycle-to-cycle standard deviation (c) as a function of the firing frequency f_{tube} for a blockage ratio of $\beta = 0.9$.

For all applied firing patterns, the detonation velocity decreases with increasing firing frequency. This can well be explained by the observed decrease in fuel supply pressure resulting in a decrease in equivalence ratio of the injected fuel–air mixture. However, only a small variation in u_{det} is observed for a given firing frequency when varying the firing pattern. The observed change in propagation velocity with frequency has thus no effect on the investigation of different firing patterns. Examination of measurement data from experiments with blockage ratios of 0.7, 0.5, and 0 revealed similar results. As the pressure amplitude of the shocks exiting the PDC tubes is directly linked to the propagation velocity of the detonation, the decrease of u_{det} with increasing firing frequency induces a decrease in the shock amplitude. This decrease in the excitation amplitude of pressure fluctuations in the plenum has to be considered

when comparing the measured pressure oscillations for different firing frequencies.

The measured detonation velocities normalized by the calculated CJ velocity, as shown in Fig. 5b, reveal that CJ detonations were observed in all measurements. The small relative standard deviation shown in Fig. 5c, indicates a repeatable operation of the PDC, resulting in comparable propagation velocities of the detonation front in all conducted cycles. However, there is a discrepancy of approximately 5 % between the actual velocities and the respective CJ velocity. We explain this by two aspects of measurement uncertainty. First, the accuracy of the applied correlation between the fuel supply pressure and the injected fuel mass flow rate is limited. The underlying correlation was derived from preliminary measurements of the stationary fuel mass flow rate for constantly open fuel valves. This implies an uncertainty in the calculated fuel mass flow rates for the periodic fuel injection during the operation of the multi-tube PDC. Second, the accuracy of the determination of the detonation velocity from the time-of-flight is limited to ±27 m/s due to the sampling rate of 1 MHz. Despite the mentioned systematic measurement uncertainties, the small cycle-to-cycle standard deviation, as shown in Fig. 5c, indicates that the operation of the multi-tube PDC allows for repeatable excitation of the pressure fluctuations in the annular plenum.

B. Prediction of Acoustic Eigenmodes and Eigenfrequencies

Numerical solution of the acoustic Helmholtz equation allows for the prediction of eigenmodes and eigenfrequencies in the annular plenum, which supports the evaluation of measured pressure fluctuations. A sketch of the examined geometry is given in Fig. 6a. The numerically predicted acoustic modes and the respective eigenfrequencies are visualized in Fig. 6b to e. The figures sketch the spatial distribution of the absolute value of the eigenmodes $|\Psi_{l,m}|$ inside one half of the annular plenum normalized by the respective maximum value. Large amplitudes in pressure oscillation are represented by red color, while blue areas indicate pressure nodes. The circular blue area on the front plane, which is visible for all eigenmodes, denotes a constant pressure due to the set acoustic boundary condition at the open outlet. The longitudinal mode number l determines the number of pressure nodes along the tube axis. The azimuthal distribution of $|\Psi_{l,m}|$ contains $2m$ pressure nodes along the entire circumference, of which only half is visualized in Fig. 6.

The accuracy of the calculations is limited due to simplified assumptions, e.g. zero pressure fluctuation at the open outlet area and constant initial temperature, when compared to the complex propagation and interaction of pressure waves in the experiment. However, the calculated eigenmodes and the respective eigenfrequencies may be used to assess possibly excited acoustic modes due to PDC operation. In the following measured pressure data at the outer wall of the plenum are analyzed and compared with the calculation results.

C. Examination of Measured Pressure Oscillations

The obtained PSD for the operation with firing pattern **I+**, $f_{\text{tube}} = 16.7\,\text{Hz}$, and $\beta = 0.9$ is shown in Fig. 7. Modes with $m = 0$ are characterized by constant $|\Psi_{l,m}|$ in the azimuthal direction, as visualized in Fig. 6b. Modes with $m > 0$ contain at least one maximum over the circumference allowing for standing or spinning modes to establish. In this work, the oscillation mode can be determined for $m = 1$ and $m = 2$. A positive value of m represents a spinning mode in positive azimuthal direction, while a negative value of m indicates a rotation in the opposite direction. A standing mode would result in equal amplitudes for positive and negative values of m. The vertical lines in Fig. 7 represent the calculated eigenfrequencies $f_{l,m}$.

All dominant peaks of the PSD, shown in Fig. 7, are linked to the acoustic eigenfrequencies of the annular plenum. However, these peaks do not match perfectly with the calculated values of $f_{l,m}$. Rather, the frequencies that correlate with peaks in the PSD can be deduced from the firing frequency of the PDC tubes and the applied firing pattern. In particular, the peak frequencies can be calculated from

$$f_{\text{peak}} = \left(k + \frac{m}{N}\right) f_{\text{eff}}, \tag{11}$$

with $k \in \mathbb{N}$. For $m = 0$, standing modes with an oscillation frequency of an integer multiple of f_{eff} are obtained. This results in a maximum pressure at the plenum inlet plane each time a PDC tube is fired, and thus leads to the excitation of the respective acoustic mode. For positive values of m, spinning modes with positive rotation direction with respect to θ are observed. The rotation velocity for spinning modes depends on k and can exceed the succession of firing PDC tubes significantly. The exact value of the angular frequency is given by $\omega = 2\pi f_{\text{peak}}$ and results in a pressure maximum at the plenum inlet matching the azimuthal position of a firing PDC tube. The PSD shown in Fig. 7 indicate that the peak amplitudes depend on the difference between f_{peak} and the nearest predicted eigenfrequency. When this deviation is small enough, the respective pressure oscillation is amplified, resulting in a large peak amplitude. For peak frequencies far off the closest predicted eigenfrequency, the associated acoustic mode is damped leading to a small amplitude in $\hat{p}_m$.

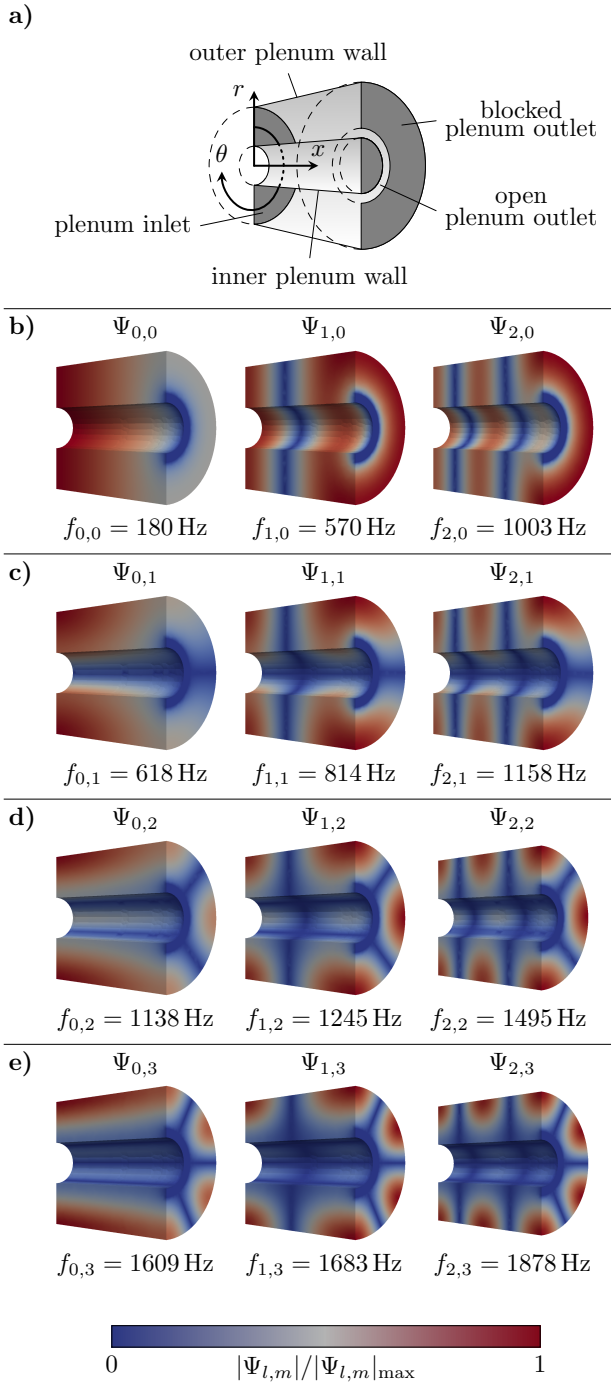

Fig. 6 Predicted acoustic eigenmodes $\Psi_{l,m}$ and the respective eigenfrequencies $f_{l,m}$ for a blockage ratio of β = 0.9. Pressure nodes are visualized by blue color, while red areas represent high oscillation amplitudes.

The spectrum for $m = 0$ (Fig. 7c) contains a dominant peak at 500 Hz. This implies a high-energy pressure oscillation at this frequency with homogeneous pressure distribution in azimuthal direction, which are excited by PDC operation with firing pattern **I+**. Additionally, peaks at 200 and 1000 Hz represent pressure fluctuations with larger amplitudes than neighboring peaks, respectively. The three frequencies are close to the the calculated eigenfrequencies $f_{0,0}$, $f_{1,0}$, and $f_{2,0}$, which suggests that the pressure oscillations correspond to the respective modes that are shown in Fig. 6b. To

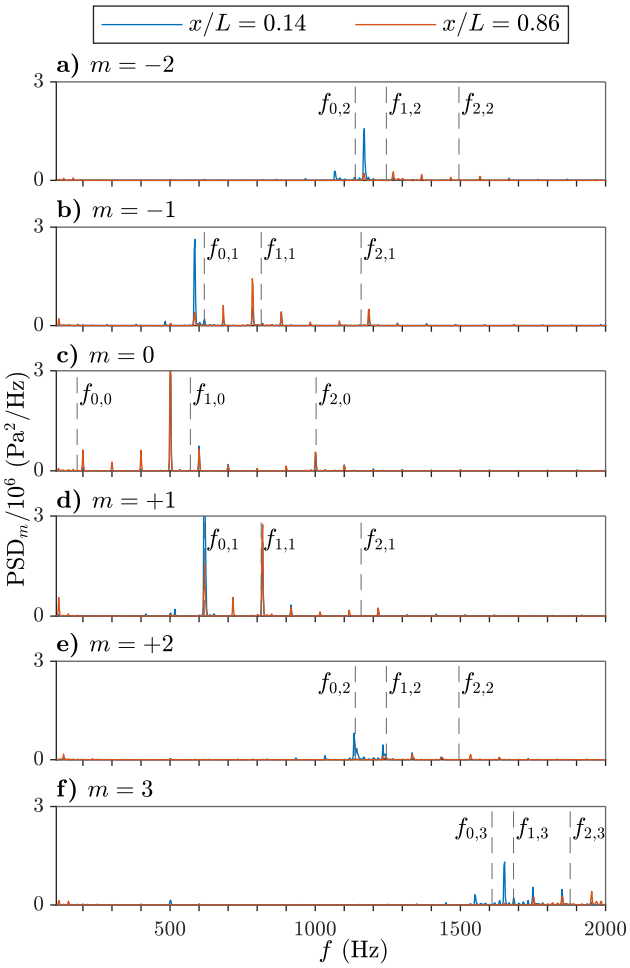

Fig. 7 PSD obtained from azimuthal frequency decomposition for firing pattern I+, $f_{\mathrm{tube}} = 16.7$ Hz, and $\beta = 0.9$ at two different axial positions x/L. The predicted eigenfrequencies $f_{l,m}$ are represented by vertical, dashed lines.

evaluate how the predicted modes are related to the measurements, we compare the axial distribution of the spatial mode shapes in Fig. 8. For this, the signals of the five axially distributed pressure sensors P51 to P55 are Fourier transformed and the amplitudes of each sensor are compared against the model at the different axial locations. The chosen frequencies match the positions of the dominant peaks in PSD($\hat{p}_0$), shown in Fig. 7c. The axial distribution of the pressure amplitude for the first three axial modes for $m = 0$ are evaluated at the plenum outer wall ($r = r_o$) and the azimuthal position of tube 5 ($\theta = 0$).

The predicted pressure amplitude of $|\Psi_{0,0}|$ shows a monotonic decrease from the inlet of the plenum ($x/L = 0$) towards the plenum outlet ($x/L = 1$). The measured amplitudes of pressure fluctuations at 200 Hz show a distinct maximum at $x/L = 0.32$. For all other axial positions, a nearly constant value of $\hat{p}$ is obtained. This mismatch between the measurement data and the predicted mode shapes can be explained by the superposition of the acoustic mode $\Psi_{0,0}$ with periodic shock structures that are emitted from the PDC outlet at a frequency of $f_{\mathrm{eff}} = 100$ Hz. The measured amplitudes for pressure oscillations at a frequency of 500 Hz show a minimum at $x/L = 0.5$ with increasing values towards the inlet and outlet of the plenum, respectively. For $f = 1000$ Hz, two minima at $x/L = 0.14$ and $x/L = 0.68$ are observed with a maximum amplitude at $x/L = 0.5$. The axial positions of the obtained extrema from the measured pressure signals agree fairly well with the model predictions. At the plenum outlet, the predicted amplitude exceeds the measured value, which is very likely to result from variations in the outlet boundary conditions between the calculations and the measurements, e.g. the flow velocity is neglected in the calculations. Other deviations between the experimental and calculated mode shapes may result from the underlying assumptions and limitations of the performed calculation. In

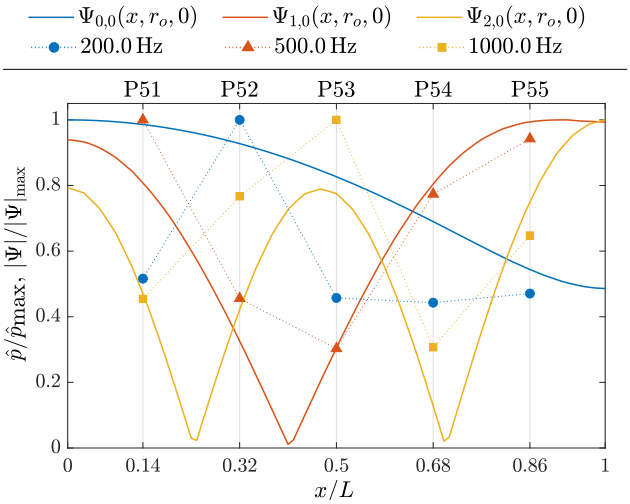

Fig. 8 Absolute value of the eigenmodes $\Psi_{l,0}$ and amplitude of measured pressure oscillation at 200, 500, and 1000 Hz as a function of the axial position x/L for firing pattern I+, $f_{\mathrm{tube}} = 16.7$ Hz, and $\beta = 0.9$. All graphs are normalized by their maximum value.

particular, the temperature inside the plenum is assumed to be steady, which is inaccurate due to fluctuating temperature variation inside the plenum caused by hot combustion products. In addition, the acoustic Helmholtz equation implies the pressure fluctuations to be small in comparison to the initial state, which is partially not given in the experiments. Nevertheless, a clear correlation between the modal predicted mode shapes and the measured pressure amplitude at the respective frequency is visible in Fig. 8. Hence, the firing pattern **I+** is capable of exciting axisymmetric acoustic modes.

The spectrum for $m = +1$ in the azimuthal frequency decomposition, shown in Fig. 7d, contains dominant peaks at 616.7 and 816.7 Hz. The largest amplitude in the respective PSD near $f_{2,1}$ is observed at 1216.7 Hz. Analogue to $m = 0$, these frequencies are correlated to the calculated eigenfrequencies $f_{l,1}$. Comparing the amplitude of the eigenmodes to the measured amplitudes for pressure oscillations at the respective frequencies for pressure sensors P51 to P55, shown in Fig. 9, reveals that the observed peaks in the azimuthal frequency decomposition are associated to the eigenmodes $\Psi_{l,1}$. The agreement between the axial distribution of the measured amplitude and the absolute value of the eigenmodes at the outer wall of the plenum is even more pronounced than for $m = 0$ (shown in Fig. 8). The deviation of the obtained amplitudes from the measured pressure and the predicted eigenmode $\Psi_{0,1}$ close to the plenum outlet is once again a result of the inaccurate choice of outlet boundary conditions in the calculations, which mainly result from two aspects. First, a mean flow velocity of $\bar{u}_{\mathrm{flow}} = 0$ m/s is assumed in the numerical calculation, which is obviously not the case for the PDC experiments. Moreover, shock waves are emitted periodically from the PDC tubes. While these shock waves result in a transient pressure at the plenum outlet, a steady pressure is assumed for the numerical model. Despite the mentioned deviations in the amplitude close to the plenum outlet, the locations of extrema are close for the predicted eigenmodes and measurements, which indicates that the operation of the multi-tube PDC with firing pattern **I+** evokes the excitation of spinning acoustic modes with $m = +1$.

Analogue considerations can be performed to explain the peaks in the PSD for $m = +2$, $m = 3$, $m = -1$, and $m = -2$ (not shown for brevity). The results clearly indicate that all observed dominant peaks are linked to acoustic eigenmodes of the annular plenum.

When considering the firing pattern **II+**, the excitation of the plenum acoustics become symmetric due to the synchronous firing of two opposite PDC tubes. This results in peaks with large amplitudes in the PSD obtained from azimuthal frequency decomposition only appearing for even values of m, as shown in Fig. 10. For $m \in [-1, +1, 3]$, only negligible amplitudes are observed. As already discussed in the previous evaluations, peak frequencies are given by Eq. 11. Besides peaks at low frequencies, which can be attributed to higher harmonics of the effective firing frequency f_{eff}, maximum amplitudes are observed at 550 and 1050 Hz, which are close to the calculated eigenfrequencies $f_{1,0}$ and $f_{2,0}$. Analogue to firing pattern **I+**, the evaluation of the amplitudes at the peak frequencies in the FT of the axially distributed sensors downstream of tube 5 reveal that the respective pressure oscillations can be correlated to the eigenmodes $\Psi_{1,0}$ and $\Psi_{2,0}$ (not shown for brevity).

For $m = \pm 2$, peaks are observed close to the eigenfrequencies $f_{0,2}$ and $f_{1,2}$. Qualitatively comparing the azimuthal

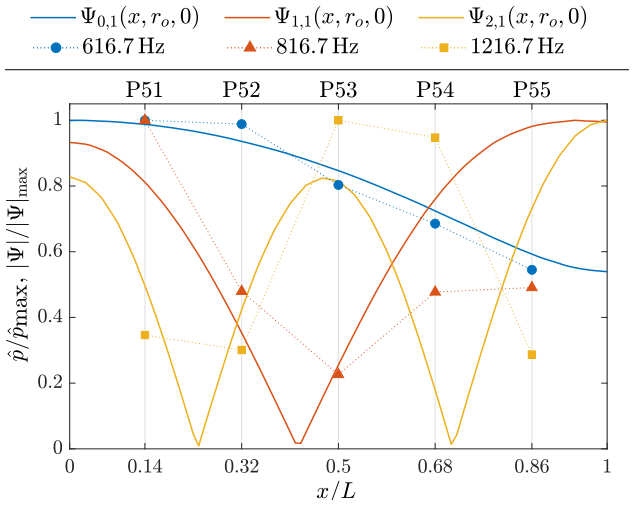

Fig. 9 Absolute value of the eigenmodes $\Psi_{l,1}$ and amplitude of measured pressure oscillation at 616.7, 816.7, and 1216.7 Hz as a function of the axial position x/L for firing pattern I+, $f_{\mathrm{tube}} = 16.7$ Hz, and $\beta = 0.9$. All graphs are normalized by their maximum value.

frequency decomposition for firing pattern **I+** (Fig. 7) and **II+** (Fig. 10) suggests that a larger number of modes is excited for sequential firing. However, quantitative comparisons are challenging. For this purpose, the non-dimensional frequency $\zeta \in [-0.5, 0.5[$ is introduced. This allows for the determination of a condensed version of the PSD obtained from azimuthal frequency decomposition $\hat{q}_m(\zeta)$ by normalizing the frequency f by the effective firing frequency f_{eff}. By this, peaks of spinning or standing acoustic modes with similar azimuthal distribution of Ψ collapse. The spectra $\hat{q}_m$ therefore give information on the energy of acoustic modes for a given azimuthal mode number m. Furthermore, the introduction of the non-dimensional frequency ζ allows for a quantitative comparison of data obtained from measurements with differing firing frequency or firing pattern. A schematic of the applied algorithm is shown in Fig. 11 for an arbitrary azimuthal mode number m.

First, the respective PSD is split into segments $\mathrm{PSD}_{m,k}(f)$ with an individual length of f_{eff}. A number of K segments is evaluated, with K being the largest integer with $K f_{\mathrm{eff}} < 5$ kHz. For each segment with $1 \leq k \leq K$, the non-dimensional frequency $\zeta = f/f_{\mathrm{eff}} - k$ is determined. The values of $\hat{q}_m(\zeta)$ are then calculated by

$$\hat{q}_m(\zeta) = f_{\mathrm{eff}} \sum_{k=1}^{K} \mathrm{PSD}_{m,k}(f)\,. \tag{12}$$

This methodology ensures the preservation of the integral energy. Lastly, the values of ζ are corrected to fit the range of $[-0.5, 0.5[$. This is achieved by increasing values smaller than -0.5 by one. The resulting distributions $\hat{q}_m(\zeta)$ are shown in Fig. 12 for sequential firing of the PDC tubes.

For firing pattern **I+**, the obtained results show pronounced peaks for $\zeta_{\mathrm{peak}} = \frac{m}{N}$. For a negative rotation orientation in θ of the firing pattern (**I−**), peaks are observed at $\zeta_{\mathrm{peak}} = -\frac{m}{N}$. Hence, the spinning direction of the excited modes depend on the rotation direction of the firing pattern. The obtained peak amplitudes for a given value of ζ_{peak}, however, are equal for firing patterns **I+** and **I−**, as shown in Fig. 12 for a firing frequency of 16.7 Hz. The evaluation of $\hat{q}_m(\zeta)$ does not allow for differentiating between longitudinal modes but rather represents the total amplitude of all acoustic modes with the respective azimuthal mode number m. When comparing the obtained distributions for varying firing frequency, it can be stated that the choice of f_{tube} does not affect the obtained spectra $\hat{q}_m$ for most values of m. For $m = 0$ and $m = +1$, however, maximum amplitudes are obtained for $f_{\mathrm{tube}} = 16.7$ Hz. This can be explained by large-amplitude pressure oscillations due to the excitation of the acoustic eigenmodes $\Psi_{1,0}$, $\Psi_{0,1}$, and $\Psi_{1,1}$, as discussed earlier. Other investigated firing frequencies result in the values of f_{peak} to differ from the acoustic eigenfrequencies of the annular plenum, leading to smaller amplitudes. Besides, for all evaluated firing frequencies the maximum value of $\hat{q}_m$ decreases with increasing absolute value of m. The largest pressure oscillations are observed for homogeneous pressure distribution in the azimuthal direction, which is associated only with longitudinal modes. Co-rotating ($m = +1$) and counter-rotating ($m = -1$) mode shapes with one azimuthal maximum contain approximately the same density of energy indicated by similar maximum values of $\hat{q}_{+1}$ and $\hat{q}_{-1}$. The same statement holds for modes with $m = \pm 2$.

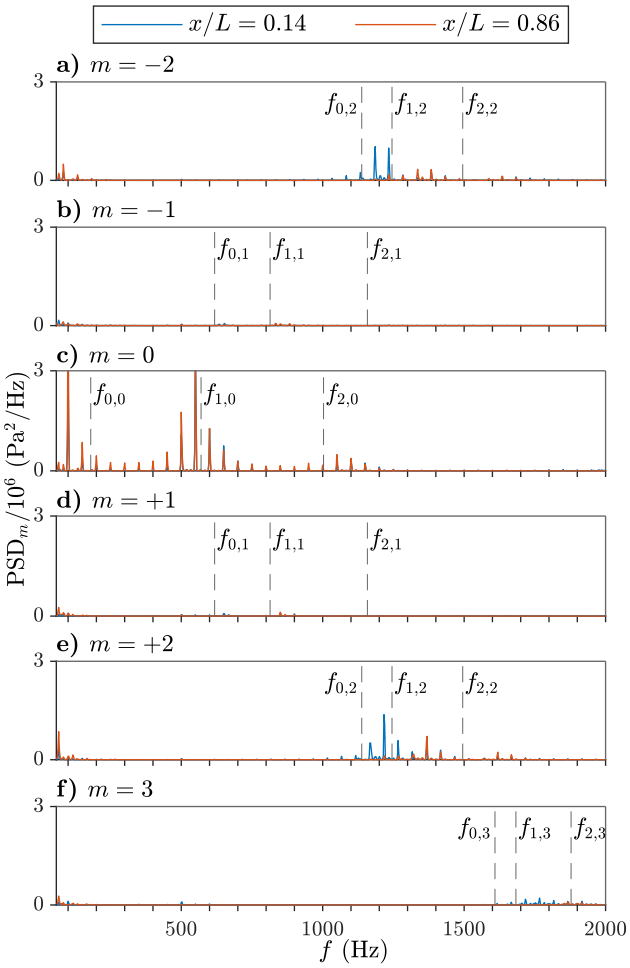

Fig. 10 PSD obtained from azimuthal frequency decomposition for firing pattern II+, $f_{\mathrm{tube}} = 16.7$ Hz, and $\beta = 0.9$ at two different axial positions x/L. The predicted eigenfrequencies $f_{l,m}$ are represented by vertical, dashed lines.

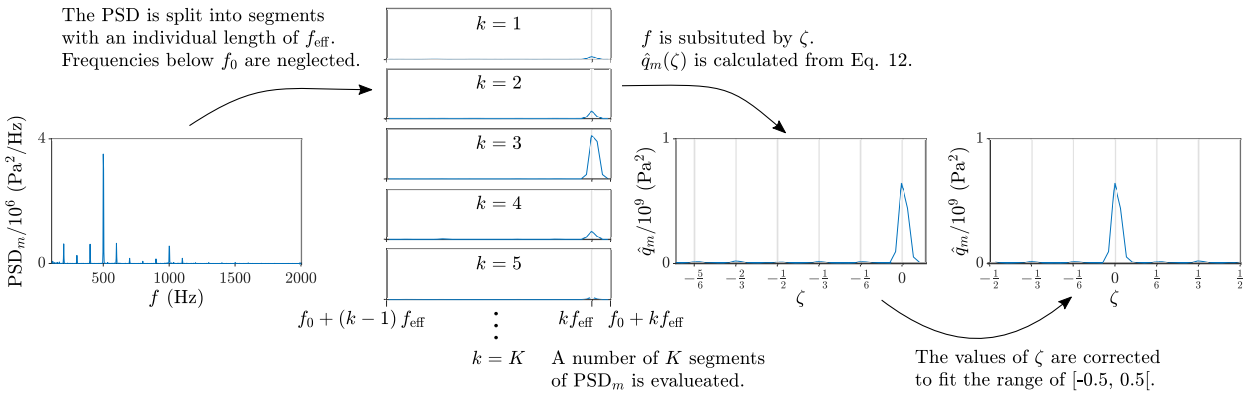

Fig. 11 Methodology for the calculation of the normalized PSD $\hat{q}_m$ (ζ).

The spectra $\hat{q}_m$ for firing pattern **II+** are shown in Fig. 13. The data reveal maxima in $\hat{q}_m$ at $\zeta \in [-1/3, 0, 1/3]$. According to the findings from Fig. 10, these values of ζ indicate the excitation of acoustic modes with $m \in [-2, 0, 2]$. The symmetric operation of opposing PDC tubes only excited acoustic modes, where pressure oscillations at θ and $\theta + \pi$

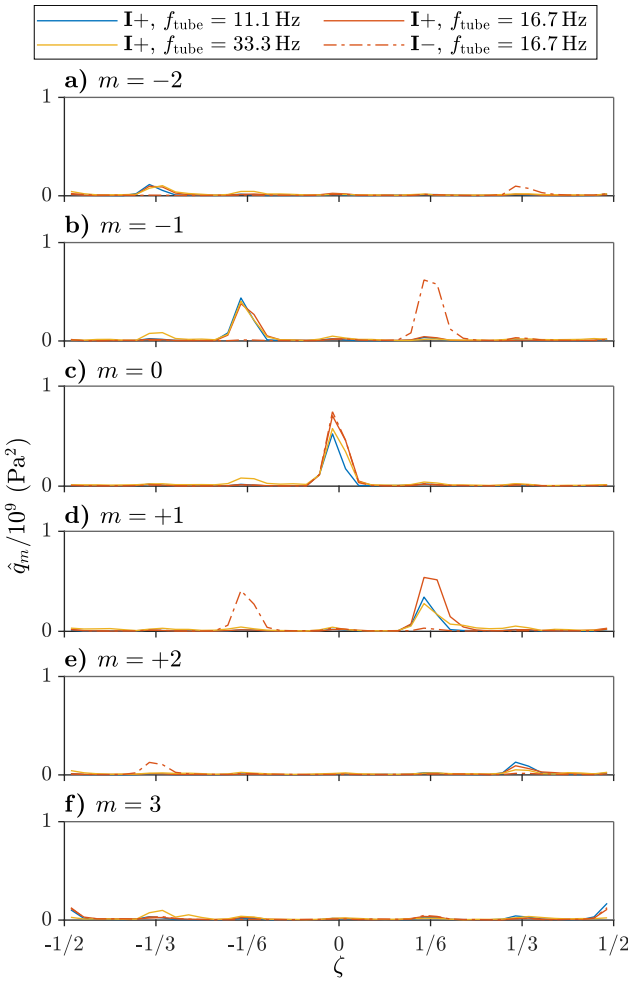

Fig. 12 Normalized PSD as a function of the non-dimensional frequency ζ for firing patterns I+ and I−.

are in phase. Hence, acoustic modes with an odd azimuthal mode number are not excited by the operation with firing pattern **II+**. Similar to the findings when operating with firing pattern **I+**, the peak amplitudes obtained for $m = -2$ and $m = +2$ are equal, indicating that both, co-rotating and counter-rotating modes are present. Furthermore, the pronounced peak amplitudes indicate, that the applied firing frequency does not affect the distribution of energy over the different azimuthal mode numbers. In order to further investigate this outcome, the measured pressure fluctuations are examined with respect to the contained integral energy and the number of dominant modes.

D. Distribution of Integral Energy over the Modes

The evaluation of the measurement data revealed that the operation of a multi-tube PDC results in the excitation of multiple acoustic modes. The observed longitudinal and azimuthal modes depend on the firing pattern and the acoustic eigenmodes of the annular plenum. As the acoustic modes cause pressure oscillations across the entire annular plenum, the amplitude as well as the integral value of pressure fluctuations at the plenum outlet is a function of the number and the amplitude of excited acoustic modes. Therefore, two quantities are determined in this work from the cumulative PSD with

$$\text{PSD}_{\text{cum}}(f) = \sum_{m=-2}^{3} \text{PSD}_m(f) \tag{13}$$

in order to quantitatively compare the measured pressure oscillations depending on operation parameters and the outlet blockage ratio. First, the integral value of PSD_{cum} is calculated as a measure of the integral energy of acoustic pressure oscillations. Second, the number of dominant modes is deduced to examine the distribution of the integral energy on the

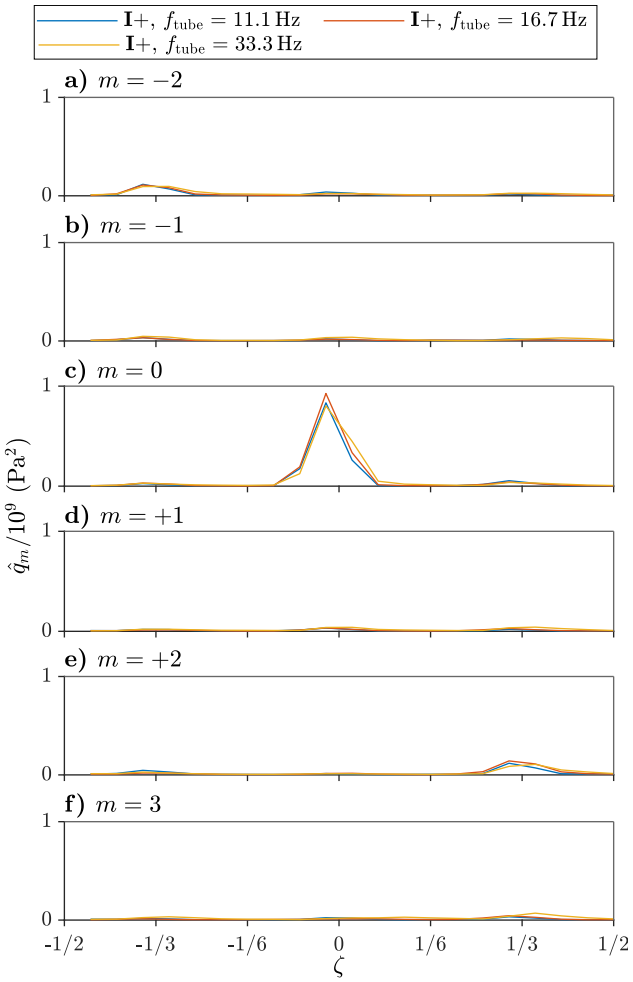

Fig. 13 Normalized PSD as a function of the non-dimensional frequency ζ for firing pattern II+.

excited modes.

In order to estimate the integral energy contained in the excited acoustic waves we compute e as the integral value of the cumulative PSD according to

$$e = \int_{f_0}^{\infty} \text{PSD}_{\text{cum}}\,(f)\ \text{d}f. \tag{14}$$

Analogue to the determination of the normalized azimuthal frequency decomposition $\hat{q}_m\,(\zeta)$, the value of f_0 is set to $f_{\text{eff}} + 1/2\ f_{\text{tube}}$ for all considered measurements to neglect the pressure fluctuations initiated by the leading shock waves emanating from the PDC tubes. The comparison of e for various firing patterns as a function of the firing frequency f_{tube}, shown in Fig. 14a, indicates that an increase in the number of simultaneously operated PDC tubes leads to an increase in integral energy. We explain this by an increasing number of simultaneously firing tubes hindering the expansion of the shock fronts in azimuthal direction, and thus, promoting larger shock amplitudes at the plenum outlet. The partial reflection at the blocked outlet area eventually results in a fraction of the contained energy to remain inside the plenum. This effect is most pronounced for firing pattern **VI**, which coincides with the largest value of e for this pattern. In addition, e increases slightly with increasing f_{tube}, which can be explained by the increasing fuel consumption rate. However, the observed increase is not proportional to the firing frequency, which is likely caused by the decrease in shock amplitude exiting the PDC tubes for increasing firing frequency due to the decrease in detonation velocity, as shown in Fig. 5a. Furthermore, there is no monotonic increase in e with increasing f_{tube}, which can be most likely attributed to the congruence of $f_{l,m}$ and f_{peak}, of which the latter depends on both, the firing frequency and the firing

pattern.

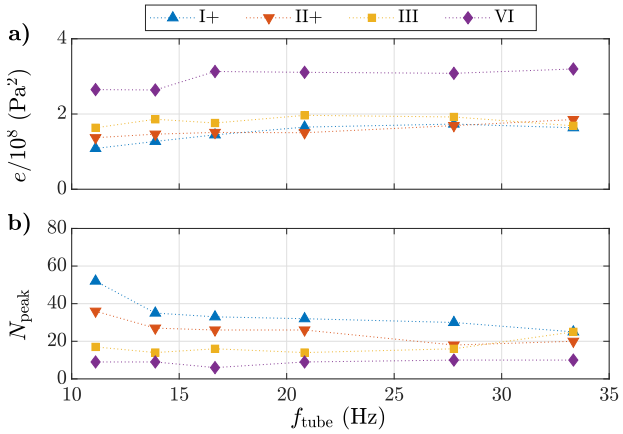

Fig. 14 Integral value of the cumulative PSD and number of dominant acoustic modes N_{peak} as a function of the firing frequency f_{tube} for $\beta = 0.9$.

Besides the integral energy, the number of acoustic modes with large oscillation amplitude as a measure of the distribution is relevant for the pressure fluctuations at the outlet of the annular plenum. A maximum pressure fluctuation is expected in case the entire acoustic energy is concentrated in one single acoustic mode. Distribution of the energy on a large number of modes would instead lead to overall smaller amplitudes in pressure fluctuations. The quantity N_{peak} denotes the number of peaks that contain 75 % of the integral energy e. A large value of N_{peak} denotes a broad distribution of the acoustic energy, whereas a small value indicates a small number of dominant modes. The values of N_{peak} as a function of the firing frequency are shown in Fig. 14b for $\beta = 0.9$ and for firing patterns **I+**, **II+**,**III**, and**VI**. A maximum number of excited acoustic modes is observed for subsequent firing of the tubes (pattern **I+**). When reducing the number of simultaneously operated PDC tubes, the number of excited azimuthal modes increases. For an increasing firing frequency the value of N_{peak} decreases. We explain this by the simultaneous increase in f_{eff}, which causes a larger difference between the values of f_{peak} (Eq. 11). Hence, fewer peaks are observed in the PSD, which eventually results in a smaller number of excited acoustic modes. Due to the reduced value of N_{peak} at small firing frequencies when increasing the number of simultaneously operated tubes, this effect is most pronounced for firing pattern **I+**.

The integral energy, shown in Fig. 15a for all applied values of β as a function of the firing frequency, indicate that increasing the blockage ratio leads to larger value of e. This effect can be attributed to a decrease in the outlet area, which hinders the dissipation of energy through the open plenum outlet. Thus, the acoustic energy in the plenum is more preserved resulting in larger values of e in multi-cycle operation of the PDC. Note, that the data for $\beta = 0.9$ are equal to the data presented in Fig. 14 for firing pattern **I+**. The results shown in Fig. 15b, reveal that a variation in the applied plenum blockage ratio with $\beta > 0$ does not affect the number of excited modes significantly. However, larger values of N_{peak} are visible for a completely open plenum outlet for most firing frequencies. In combination with the small integral energy for $\beta = 0$, this indicates that small-amplitude pressure oscillations are obtained for this configuration.

In conclusion, a small number of simultaneously firing PDC tubes and the decrease in blockage ratio leads to a reduced integral energy and an increased number of modes to which it is distributed. Besides, an increase in firing frequency causes an elevated integral energy. The smallest integral energy of acoustic pressure oscillations and the largest number of excited acoustic modes were found for the sequential firing of the PDC tubes (firing pattern **I+**) at a firing frequency of $f_{tube} = 11.1$ Hz. The integral energy e was found to increase for larger firing frequencies. However, the integral energy is not the only parameter of interest for choosing a suitable PDC operating condition. For instance, the integral energy e can be normalized with the fuel consumption rate, which is proportional to f_{tube}. The resulting normalized acoustic oscillations decrease, in contrast to the integral energy e, with increasing firing frequency. As indicated by partly non-monotonic distributions of e and N_{peak}, the proper adjustment of the PDC operation parameters with regard to the eigenfrequencies of the plenum is recommended in order to achieve minimum pressure fluctuations at the turbine inlet due to acoustic modes.

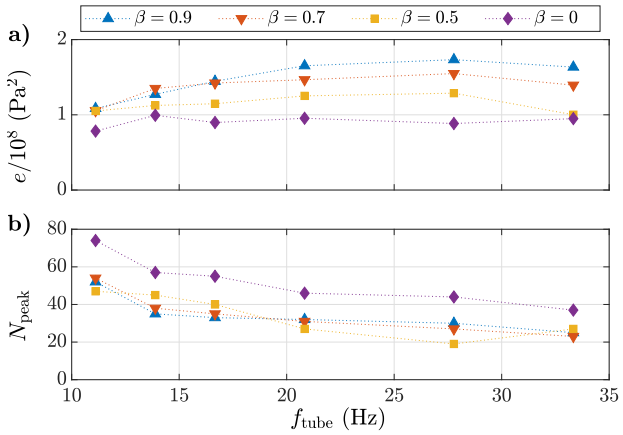

Fig. 15 Integral value of the cumulative PSD and number of dominant acoustic modes as a function of the firing frequency f_{tube} for firing pattern I+.

IV. Conclusion

A pulse detonation combustor consisting of six tubes connected to an annular plenum was operated with various firing frequencies and firing patterns. Furthermore, the plenum outlet blockage was varied to reproduce the influence of an attached turbine. Recorded pressure traces in the plenum revealed considerable pressure oscillations during the entire operation duration in addition to the expected pressure peaks subsequent to the firing of the PDC tubes. As conventional turbines are designed for stationary inlet conditions, these oscillations are expected to have negative effect on the turbine performance. Therefore, this work focuses on the origin of these fluctuations as well as their dependence on operation parameters and acoustic boundary conditions at the plenum outlet by the examination of pressure histories at different axial and azimuthal positions in the plenum.

Numerical simulations of the homogeneous acoustic Helmholtz equation were conducted to predict the acoustic eigenmodes and the corresponding eigenfrequencies of the annular plenum. Azimuthal frequency decomposition was performed using the signals of six circumferentially distributed flush mounted pressure sensors at the outer plenum wall. The resulting power spectral density showed dominant peaks at frequencies close to the predicted eigenfrequencies. The evaluation of pressure signals at five different axial positions confirmed that the associated pressure oscillations in the plenum correspond to the acoustic eigenmodes. By normalizing the frequency it was demonstrated that the observed peaks in the azimuthal frequency decomposition arise from rotating acoustic modes. The respective rotation frequencies were found to depend on the azimuthal mode number, the firing frequency, and the firing pattern. Furthermore, it was found that the maximum pressure in azimuthal direction occurs at the position of the firing tube regardless of the operation mode.

A quantitative comparison of pressure oscillations for varying firing frequency revealed that the amplitudes of excited acoustic modes increase with increasing firing frequency due to an elevated fuel consumption rate. Furthermore, the integral energy was determined from the cumulative PSD of all investigated azimuthal mode numbers. A decreasing number of simultaneously firing PDC tubes as well as a smaller blockage ratio at the plenum outlet were found to decrease the energy of the acoustic oscillations. Simultaneously, the number of acoustic modes, to which the acoustic energy is distributed, increases, leading to smaller individual amplitudes of the acoustic modes. In conclusion, sequential firing of the PDC tubes in combination with a small firing frequency is the favorable configuration for achieving small acoustic pressure fluctuations at the turbine inlet.

The present study reveals that a suitable choice of the operation parameters of a multi-tube PDC, i.e. the firing pattern and the firing frequency, allows for decreasing the pressure oscillations in an annular plenum. Further reductions can be achieved by the appropriate design of the transition section between the plenum and the turbine. In particular, the presence of a turbine results in a partly blocked plenum outlet inducing modified acoustic boundary conditions when compared to the experiments presented in this work. Based on the findings of the present study, this is expected to result in an increased energy contained by acoustic pressure oscillations in the plenum. Besides, the acoustic eigenmodes and the corresponding eigenfrequencies vary, which should be considered during the choice of operation parameters for the PDC in order to avoid high-amplitude pressure fluctuations at a single frequency. This resonance can also be avoided by damping mechanisms, e.g. Helmholtz resonators. By this, the excitation of certain eigenmodes is hindered, which

eventually results in smaller pressure oscillations. The results of this study allow for minimizing acoustic pressure oscillations, and thereby enhancing the overall efficiency of the pulse detonation engine.

Acknowledgments

The authors gratefully acknowledge the support of the Deutsche Forschungsgemeinschaft (DFG) as part of Collaborative Research Center CRC 1029 "Substantial efficiency increase in gas turbines through direct use of coupled unsteady combustion and flow dynamics" on projects A01 and C01. The authors also wish to thank Andy Göhrs and Thorsten Dessin for their technical support.

References

[1] Bluemner, R., Bohon, M. D., Paschereit, C. O., and Gutmark, E. J., "Single and counter-rotating wave modes in an RDC," *2018 AIAA Aerospace Sciences Meeting*, 2018, p. 1608. https://doi.org/https://doi.org/10.2514/6.2018-1608.

[2] Yücel, F. C., Habicht, F., Bohon, M., and Paschereit, C. O., "Autoignition in stratified mixtures for pressure gain combustion," *Proceedings of the Combustion Institute*, 2020. https://doi.org/https://doi.org/10.1016/j.proci.2020.07.108.

[3] Rezay Haghdoost, M., Edgington-Mitchell, D., Nadolski, M., Klein, R., and Oberleithner, K., "Dynamic evolution of a transient supersonic trailing jet induced by a strong incident shock wave," *Physical Review Fluids*, Vol. 5, No. 7, 2020, p. 073401. https://doi.org/https://doi.org/10.1103/PhysRevFluids.5.073401.

[4] Rouser, K., King, P., Schauer, F., Sondergaard, R., and Hoke, J., "Experimental performance evaluation of a turbine driven by pulsed detonations," *51st AIAA aerospace sciences meeting including the new horizons forum and aerospace exposition*, 2013, p. 1212. https://doi.org/https://doi.org/10.2514/6.2013-1212.

[5] Rezay Haghdoost, M., Edgington-Mitchell, D. M., Paschereit, C. O., and Oberleithner, K., "High-Speed Schlieren and Particle Image Velocimetry of the Exhaust Flow of a Pulse Detonation Combustor," *AIAA Journal*, Vol. 58, No. 8, 2020, pp. 3527–3543. https://doi.org/doi/abs/10.2514/1.J058540.

[6] Rezay Haghdoost, M., Thethy, B. S., Edgington-Mitchell, D., Habicht, F. E., Vinkeloe, J., Djordjevic, N., Paschereit, C. O., and Oberleithner, K., "Mitigation of Pressure Fluctuations from an Array of Pulse Detonation Combustors," *Journal of Engineering for Gas Turbines and Power*, 2020. https://doi.org/https://doi.org/10.1115/1.4049857.

[7] Rasheed, A., Furman, A. H., and Dean, A. J., "Pressure measurements and attenuation in a hybrid multitube pulse detonation turbine system," *Journal of Propulsion and Power*, Vol. 25, No. 1, 2009, pp. 148–161. https://doi.org/https://doi.org/10.2514/1.31893.

[8] Qiu, H., Xiong, C., and Zheng, L., "Experimental investigation of an air-breathing pulse detonation turbine prototype engine," *Applied Thermal Engineering*, Vol. 104, 2016, pp. 596–602. https://doi.org/https://doi.org/10.1016/j.applthermaleng.2016.05.077.

[9] Xisto, C., Petit, O., Grönstedt, T., Rolt, A., Lundbladh, A., and Paniagua, G., "The efficiency of a pulsed detonation combustor–axial turbine integration," *Aerospace Science and Technology*, Vol. 82-83, 2018, pp. 80–91. https://doi.org/10.1016/j.ast.2018.08.038, URL https://doi.org/10.1016/j.ast.2018.08.038.

[10] Fernelius, M. H., "Experimental and computational analysis of an axial turbine driven by pulsing flow," 2017.

[11] Chen, L., Zhuge, W., Zhang, Y., Li, Y., and Zhang, S., "Investigation of flow structure in a turbocharger turbine under pulsating flow conditions," *SAE International Journal of Fuels and Lubricants*, Vol. 1, No. 1, 2009, pp. 1167–1174.

[12] Hellström, F., "Numerical computations of the unsteady flow in turbochargers," Ph.D. thesis, KTH, 2010.

[13] Evesque, S., Polifke, W., and Pankiewitz, C., "Spinning and azimuthally standing acoustic modes in annular combustors," *9th AIAA/CEAS Aeroacoustics Conference and Exhibit*, 2003, p. 3182. https://doi.org/https://doi.org/10.2514/6.2003-3182.

[14] Noiray, N., and Schuermans, B., "On the dynamic nature of azimuthal thermoacoustic modes in annular gas turbine combustion chambers," *Proceedings of the Royal Society A: Mathematical, Physical and Engineering Sciences*, Vol. 469, No. 2151, 2013, p. 20120535. https://doi.org/https://doi.org/10.1098/rspa.2012.0535.

[15] Mensah, G. A., Campa, G., and Moeck, J. P., "Efficient computation of thermoacoustic modes in industrial annular combustion chambers based on Bloch-wave theory," *Journal of Engineering for Gas Turbines and Power*, Vol. 138, No. 8, 2016. https://doi.org/https://doi.org/10.1115/1.4032335.

[16] Zeleznik, F. J., and Gordon, S., "Calculation of detonation properties and effect of independent parameters on gaseous detonations," *ARS Journal*, Vol. 32, No. 4, 1962, pp. 606–615. https://doi.org/https://doi.org/10.2514/8.6080.

[17] Rienstra, S. W., and Hirschberg, A., "An introduction to acoustics," *Eindhoven University of Technology*, Vol. 18, 2004, p. 19.

[18] Schuermans, B., Paschereit, C. O., and Monkewitz, P., "Non-linear combustion instabilities in annular gas-turbine combustors," *44th AIAA aerospace sciences meeting and exhibit*, 2006, p. 549. https://doi.org/https://doi.org/10.2514/6.2006-549.

[19] Mensah, G. A., and Moeck, J. P., "Limit cycles of spinning thermoacoustic modes in annular combustors: A bloch-wave and adjoint-perturbation approach," *ASME Turbo Expo 2017: Turbomachinery Technical Conference and Exposition*, American Society of Mechanical Engineers Digital Collection, 2017. https://doi.org/https://doi.org/10.1115/GT2017-64817.